Check for updates

Geophysical Research Letters

RESEARCH LETTER
10.1029/2023GL108015

Role of Strong Sea Surface Temperature Diurnal Variation in Triggering the Summer Monsoon Onset Over the Bay of Bengal in a Climate Model

Yajuan Song[1,2,3], Xiaodan Yang[1,2,3], Ying Bao[1,2,3], Fangli Qiao[1,2,3], and Zhenya Song[1,2,3]

[1]First Institute of Oceanography, and Key Laboratory of Marine Science and Numerical Modeling, Ministry of Natural Resources, Qingdao, China, [2]Laboratory for Regional Oceanography and Numerical Modeling, Qingdao Marine Science and Technology Center, Qingdao, China, [3]Shandong Key Laboratory of Marine Science and Numerical Modeling, Qingdao, China

Key Points:

- The spurious delayed Asian summer monsoon onset (SMO) is improved by including the effect of large sea surface temperature (SST) diurnal amplitude in a climate model
- Strong diurnal variation of SST contributes to upper ocean warming in the Bay of Bengal before the Asian SMO
- Large-scale circulation with favorable conditions for convection activity in response to ocean warming triggers an advanced monsoon onset

Supporting Information:

Supporting Information may be found in the online version of this article.

Correspondence to:

Z. Song,
songroy@fio.org.cn

Citation:

Song, Y., Yang, X., Bao, Y., Qiao, F., & Song, Z. (2024). Role of strong sea surface temperature diurnal variation in triggering the summer monsoon onset over the Bay of Bengal in a climate model. *Geophysical Research Letters*, *51*, e2023GL108015. https://doi.org/10.1029/2023GL108015

Received 5 JAN 2024
Accepted 26 JUL 2024

Author Contributions:

Conceptualization: Fangli Qiao, Zhenya Song
Data curation: Xiaodan Yang, Ying Bao
Formal analysis: Yajuan Song, Zhenya Song
Funding acquisition: Zhenya Song
Investigation: Xiaodan Yang
Methodology: Yajuan Song, Zhenya Song
Project administration: Zhenya Song
Resources: Zhenya Song
Software: Xiaodan Yang, Ying Bao
Supervision: Fangli Qiao, Zhenya Song
Validation: Xiaodan Yang, Ying Bao
Visualization: Yajuan Song, Zhenya Song

© 2024. The Author(s).
This is an open access article under the terms of the Creative Commons Attribution-NonCommercial-NoDerivs License, which permits use and distribution in any medium, provided the original work is properly cited, the use is non-commercial and no modifications or adaptations are made.

Abstract The earliest Asian summer monsoon onset (SMO) occurs in the Bay of Bengal (BoB), heralding the coming of the rainy season. In late April or early May, the strong sea surface temperature (SST) diurnal variation accompanied by ocean surface warming triggers the SMO. However, this observed diurnal cycle intensity cannot be reasonably simulated by state-of-the-art climate models, resulting in a spurious delayed SMO. To address this issue, the SST diurnal cycle parameterized by a diagnostic sublayer scheme was incorporated into a climate model named FIO-ESM v2.0. The large diurnal amplitude of SST contributes to surface warming and changes atmospheric circulation. Consequently, the high-pressure anomaly at high levels and an inverted trough at low levels promote more convective activity, triggering an earlier SMO. Our findings improve the ability of climate models in simulating the evolution of the Asian monsoon system.

Plain Language Summary Asian summer monsoon onset (SMO) accompanied by the coming of the rainy season has a significant impact on the lives and livelihoods of more than half of the world's population. However, state-of-the-art climate models struggle to capture the major features of SMO accurately. The simulated diurnal amplitude of sea surface temperature (SST) is much smaller compared with observation, resulting in a cold bias in SST and a delayed SMO in the Bay of Bengal (BoB). Here, we incorporated a diagnostic sublayer parameterization into the climate model to account for the effect of a strong diurnal cycle. The SST in the BoB increases, and more convective activities are promoted in response to the warmer underlying surface. Changes in monsoon circulation create favorable environmental conditions for an advanced SMO. Considering the effect of strong diurnal variation provides a solution to reduce common biases of the climate model in simulating SMO.

1. Introduction

The onset of the Asian summer monsoon marks a critical transition from a dry and cold season to a rainy and hot season, substantially impacting the production and living of billions of inhabitants. The monsoon onset date, regarded as an intrinsic indicator of the transition of seasons, is crucial for agricultural and economic activities in the monsoon region. Increasing observations show that the Asian summer monsoon initially breaks out in the southern Bay of Bengal (BoB) in late April or early May (K. Li et al., 2018; B. Wang & LinHo, 2002; Yu, Li, et al., 2012). Convection activity then propagates eastward toward the South China Sea and westward toward India (Liu, Liu, et al., 2015; Zhu & Li, 2017), accompanied by a sudden shift in wind and a higher chance of extreme rainfall over South and East Asia.

The summer monsoon onset (SMO) in the BoB is modulated by multi-scale climatic variabilities and the mean state of the tropical pattern. In terms of interannual variability, El Niño-Southern Oscillation (ENSO) is the dominant force influencing the SMO, with the advanced (delayed) onset after the occurrence of La Niña (El Niño) events in the preceding winter and spring (He & Zhu, 2015; Mao & Wu, 2007; X. Wang et al., 2013). Besides, the tropical Pacific upper ocean heat content and convection anomalies over the southern Philippines related to ENSO substantially change the SMO in the BoB (Feng et al., 2013; Liu, Wu, & Ren, 2015). On the intraseasonal timescale, the first northward propagating intraseasonal oscillations (ISOs) trigger the SMO (K. Li, Li, et al., 2016; B. Wang et al., 2006). The relationship between ISOs and SMO is also modulated by ENSO (K. Li et al., 2018). On the synoptic timescale, tropical cyclones developed over the BOB during the monsoon transition

Writing – original draft: Yajuan Song
Writing – review & editing: Fangli Qiao, Zhenya Song

period, also known as the monsoon onset vortex (MOV), influence the SMO (Z. Li et al., 2021; Wu et al., 2011, 2013; Zhu & He, 2013). Significantly, sea surface temperature (SST) reaches its annual maximum just before the SMO, which regulates the northward propagating ISOs and the development of MOV (K. Li, Liu, et al., 2016; Shroyer et al., 2021; Wu et al., 2012). Yu, Shi, et al. (2012) found that this SST warming is likely induced by shallow mixed layer depth (MLD), weak winds, and strong solar radiation along with a strong diurnal cycle. On higher frequency timescale, such as diurnal variation, the effect of large SST diurnal amplitude on the SMO remains largely unknown.

Despite significant advances in climate modeling over the past few decades, climate models still suffer systematic biases in simulating SMO. Sperber et al. (2013) evaluated model performance in the Coupled Model Intercomparison Project phase 3 and phase 5 (CMIP3 and CMIP5), revealing that the simulated SMO in the BoB is delayed for 3 to 6 pentads in multi-model mean results. Although the models participating in the CMIP6 are more skillful in simulating the climatological features of monsoon, the SMO remains delayed over the Indian, BoB, South China Sea, and East Asia regions (Dong et al., 2016; Hu et al., 2023; H. Wang et al., 2022). For the BoB, the late SMO is associated with the local SST bias, which could lead to inconsistency between simulations and observations regarding the development of convection activity.

SST exhibits a pronounced diurnal cycle due to the periodic variation of solar radiation, particularly in the tropical region. Under low wind speeds and strong solar radiation conditions, daily mean SST increases by 2–3°C due to the strong diurnal variation (Soloviev & Lukas, 1997). Incorporating the SST diurnal cycle into a coupled model can improve the tropical cold tongue bias, with temperature changes of up to 1°C (Bernie et al., 2008). This high-frequency process is crucial for air-sea flux exchange in the climate system, but most CMIP6 climate models struggle to accurately simulate the intensity of the diurnal cycle due to the coarse vertical resolution of the ocean model and low coupling frequency between ocean and atmosphere components. Previous studies indicated that the diurnal cycle can be captured when the frequency of air-sea flux exchange is higher than 3 hr, and the vertical resolution near the surface is about 1 m (Bernie et al., 2005; Masson et al., 2012), which is still a challenge to climate models (Yang et al., 2023). Therefore, to capture the amplitude of observed SST diurnal variation, a sublayer parameterization modified by Yang et al. (2017) is introduced into the climate model. The present study intends to expand on the current understanding of the relationship between diurnal and seasonal variations, that is, to investigate the possible effect of strong diurnal variation on the SMO.

2. Model, Methods, and Data

2.1. Model

The modified sublayer parameterization was included in the First Institute of Oceanography-Earth System Model version 2.0 (FIO-ESM v2.0), a fully coupled model that participated in CMIP6. FIO-ESM v2.0 consists of six geophysical component models (Bao et al., 2020). The Community Atmosphere Model version 5 (CAM5, Neale et al., 2010) and the Community Land Model version 4.0 (CLM4.0, Lawrence et al., 2011) serve as the atmosphere and land surface components. The sea ice and runoff components are the Los Alamos National Laboratory sea-ice model version 4 (CICE4, Hunke & Lipscomb, 2008) and the River Transport Model (Branstetter, 2001), respectively. The Parallel Ocean Program version 2.0 is the ocean component (POP2.0, Smith et al., 2010). The MArine Science and NUmerical Modeling wave model is coupled with POP2.0 to consider the effects of ocean surface waves (Qiao et al., 2016).

Six geophysical components are linked by Coupler 7 (Craig et al., 2011). Specifically, the atmosphere, land surface, and sea ice components exchange data with the coupler every 0.5 hr, while the runoff, ocean, and wave models exchange data every 3 hr. The frequency of coupling between POP2.0 and other components is adequate for identifying diurnal variation. The POP2.0 has a nonuniform horizontal resolution of approximately 1.1° in longitude and 0.27°–0.54° in latitude, featuring 60 vertical levels with the first layer at 5 and 10 m intervals in the upper 150 m of the ocean. Note that this vertical resolution is inadequate for accurately modeling observed SST diurnal variation.

2.2. SST Diurnal Variation Parameterization Scheme

When heat absorption at the ocean surface exceeds heat loss, a sublayer forms near the surface. The change of SST should be equal to the temperature change at the top of that sublayer. Yang et al. (2017) proposed a sublayer

19448007, 2024, 15, Downloaded from https://agupubs.onlinelibrary.wiley.com/doi/10.1029/2023GL108015 by QINGDAO UNIVERSITY OF SCIENCE & TECH, Wiley Online Library on [09/03/2026]. See the Terms and Conditions (https://onlinelibrary.wiley.com/terms-and-conditions) on Wiley Online Library for rules of use; OA articles are governed by the applicable Creative Commons License

19448007, 2024, 15, Downloaded from https://agupubs.onlinelibrary.wiley.com/doi/10.1029/2023GL108015 by QINGDAO UNIVERSITY OF SCIENCE & TECH, Wiley Online Library on [09/03/2026]. See the Terms and Conditions (https://onlinelibrary.wiley.com/terms-and-conditions) on Wiley Online Library for rules of use; OA articles are governed by the applicable Creative Commons License

parameterization scheme based on Schiller and Godfrey (2005) and Gentemann et al. (2009)'s work, assuming that temperature decreases exponentially with depth. The difference in temperature between the top of the sublayer and the top of the model layer is parameterized as follows:

$$\Delta T(t) = \frac{I_{\mathrm{sw}}(t)}{\rho C_p}\left(S\frac{1-f_w(-D_T(t))}{D_T(t)} + \frac{\partial f_w(z)}{\partial z} - \frac{1-f_w(-z_{k=1})}{z_{k=1}}\right) - \frac{I_{\mathrm{surf}}(t)}{\rho C_p}\left(\frac{s}{D_T(t)} - \frac{1}{z_{k=1}}\right) \quad (1)$$

where $S = D_T(t)/\int_0^{D_T} e^{-9.5(z/D_T)^a}$, D_T is sublayer depth, ρ is the seawater density, c_p is the volumetric heat capacity, I_{sw} and I_{surf} are the integrals of the shortwave radiation flux and surface heat fluxes, and f_w is the penetration of the shortwave radiation in the ocean.

The temperature difference $\Delta T(t)$, which is re-calculated at each time step and each spatial location, is added to SST at the first model layer (at 5 m) to represent SST at 0 m, then sent to the coupler to calculate heat flux and change the air-sea interaction processes. Only the potential temperature variable contains 61 layers vertically. More details about the sublayer parameterization scheme are illustrated in Yang et al. (2017) and Bao et al. (2020).

2.3. Experiments

To investigate the impact of the strong diurnal cycle on the SMO, two comparative experiments were conducted. The first experiment, denoted as Exp_WDA, did not consider the sublayer parameterization scheme, resulting in a *weak* simulated diurnal variation with a small amplitude. In contrast, the second experiment, denoted as Exp_SDA, incorporated the sublayer parameterization scheme, resulting in a *strong* simulated diurnal variation with a large amplitude. Two experiments were initialed from an equilibrium initial state anchored in preindustrial time at 300 years and integrated with all forcings prescribed from 1850 to 2014, the same as the historical experiment in CMIP6 (Eyring et al., 2016). The performance of FIO-ESM v2.0 was evaluated before conducting two experiments. The climatological pattern of SST, precipitation, and ENSO were reasonably simulated (Bao et al., 2020; Deepthi & Sivakumar, 2022). Additionally, the mean state of the monsoon system and mechanical and thermal forcings of Asian orography were well reproduced by FIO-ESM v2.0 (J. Li et al., 2023; Song et al., 2020).

2.4. Data

High temporal resolution SST data are derived from the daily Optimum Interpolation Sea Surface Temperature (OISST v2) data set for the period of 1982–2014 based on the measurements from the Advanced Very High-Resolution Radiometer satellite data (Huang et al., 2021), the African-Asian-Australian Monsoon Analysis and Prediction (RAMA) mooring data set at (15°N, 90°E) and (12°N, 90°E) for the period of 2009–2014 (McPhaden et al., 2009), and the fifth generation ECMWF reanalysis (ERA5) for the period of 1979–2014. Despite the high time frequency in ERA5, there are no variations due to the diurnal variations in SST (Hersbach et al., 2020).

The hourly wind data at 10 m, sourced from the ERA5 between 1979 and 2014, is utilized to investigate the time of SMO in the BoB. Daily NOAA interpolated outgoing longwave radiation (OLR) products spanning from 1979 to 2014 are used as a proxy for large-scale convective activity over the BoB (Chelliah & Arkin, 1992).

3. Results

3.1. Variation of SST During Monsoon Onset

The composite time series of SST before and after the SMO in the BoB are presented in Figure 1. Here the local SMO date is determined according to the criteria proposed by Yu, Li, et al. (2012): the area-averaged OLR in the BoB (7.5°N–12.5°N, 85°E–95°E) less than 220 W m^{-2} and the zonal wind changing from negative to positive maintaining for the subsequent 10 days (including the first day). We calculate the SMO date on each grid. To investigate the effect of diurnal variation on the SMO, we define the pre-onset and post-onset stages as the periods from 10 days before the onset day (D − 10) to the day before the onset (D − 1) and from the day after the onset day (D + 1) to 10 days after the onset (D + 10), respectively.

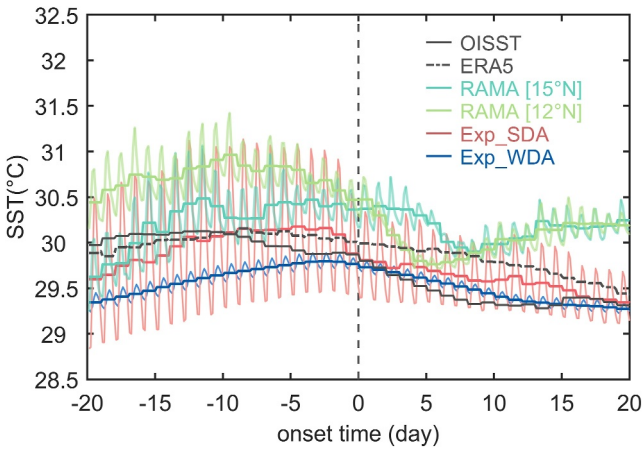

Figure 1. Composite time series of sea surface temperature during the summer monsoon onset (SMO) averaged in the Bay of Bengal region (7.5°N–12.5°N, 85°E–95°E). The zero in the *x*-axis indicates the day of SMO, and the negative (positive) value indicates the days before (after) SMO. The black lines represent Optimum Interpolation Sea Surface Temperature (solid line) and ECMWF reanalysis (dashed line) results, respectively. The dark (light) red line shows the daily (3 hr) mean result of EXP_SDA, and the dark (light) blue line shows the daily (3 hr) mean result of EXP_WDA. Observed results of the RAMA buoy array at 15°N and 12°N for the period of 2009–2014 are shown in two green lines.

Before the SMO, the area averaged SST in the BoB showed strong diurnal variation (Figure S1 in Supporting Information S1). The diurnal amplitude, which represents the intensity of diurnal variation, exceeds 1.3°C based on RAMA mooring at 15°N, and 12°N (Figure 1). However, the model cannot reasonably simulate the diurnal amplitude in Exp_WDA. The SST exhibits weak diurnal variation with a smaller diurnal amplitude of less than 0.5°C. By incorporating the sublayer parameterization scheme into the model, the diurnal amplitude increases up to 1.9°C in Exp_SDA. In the pre-onset stages, the clear skies, intense solar radiation, weak surface winds, and a shallow MLD contribute to a strong SST diurnal cycle (Wu et al., 2012). While in the post-onset stages, the large diurnal amplitude decreases rapidly due to the coming of the rainy season. Increased convective activity with a significant quantity of cloud cover reflects solar radiation and less heat is absorbed during the day.

The presence of strong diurnal variation contributes to an increase in daily mean SST. Comparing the results of two experiments, the daily mean SST in Exp_SDA with a larger diurnal amplitude is about 0.5°C warmer than it in Exp_WDA during the pre-onset stage. The maximum daily mean SST reaches up to 30°C in Exp_SDA, but lower than 30°C in Exp_WDA. Meanwhile, the RAMA SST with a larger diurnal amplitude also shows a warmer daily SST, with a maximum value up to 30.5°C. The model with strong diurnal variation has a more accurate capability to simulate the pre-onset warming SST caused by intensive diurnal processes.

The diurnal variation contributes to the increase in SST, which is crucial for the SMO. Based on the ERA5 reanalysis and NOAA OLR data sets, the SMO in the southern BOB typically occurs at the end of April or early May, during the 115th to 130th day of the year (Figure 2a). However, the simulated onset time in Exp_WDA is noticeably delayed. As shown in Figure 2d, differences between Exp_WDA and observation are approximately 10–15 days (2–3 pentads) in the central BOB and 15–20 days (3–4 pentads) in the western BoB from 10°N to 15°N. Considering the impact of strong diurnal variation in the model, the time of SMO is advanced by approximately 10–15 days (2–3 pentads) from the center to the eastern BoB, as evidenced by comparing the results of Exp_SDA with Exp_WDA (Figure 2f). The bias in SMO in the central BoB is significantly reduced (Figure 2e).

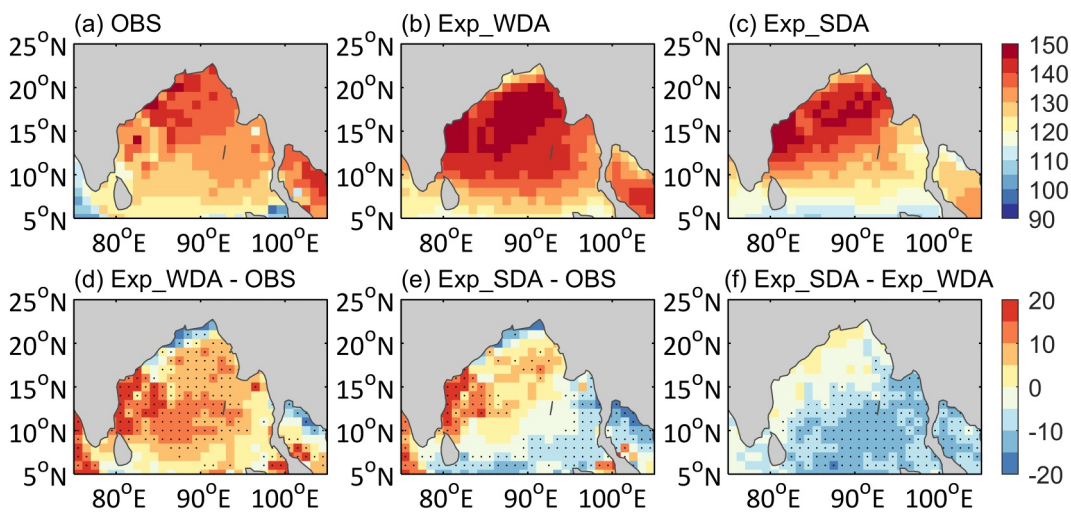

Figure 2. The summer monsoon onset time (days of the year) in (a) observation, (b) EXP_WDA, (c) EXP_SDA, and differences between (d) EXP_WDA and observation, (e) EXP_SDA and observation, and (f) EXP_SDA and EXP_WDA. The dotted areas in panels (d–f) indicate that the differences are significant at a 95% level based on the *t*-test.

19448007, 2024, 15, Downloaded from https://agupubs.onlinelibrary.wiley.com/doi/10.1029/2023GL108015 by QINGDAO UNIVERSITY OF SCIENCE & TECH, Wiley Online Library on [09/03/2026]. See the Terms and Conditions (https://onlinelibrary.wiley.com/terms-and-conditions) on Wiley Online Library for rules of use; OA articles are governed by the applicable Creative Commons License

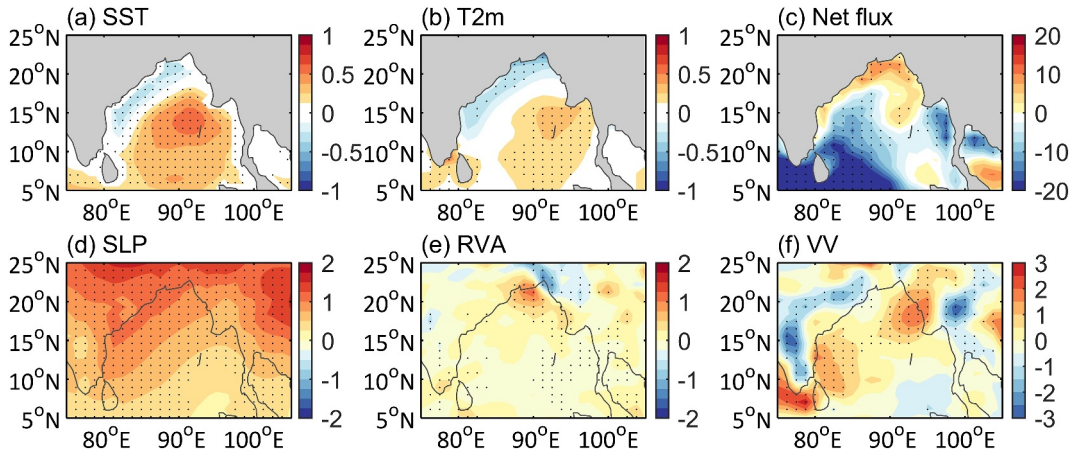

Figure 3. Composite differences between EXP_SDA and EXP_WDA in the pre-onset stage, (a) sea surface temperature (units: °C); (b) air temperature at 2m (units: °C); (c) net heat flux at the surface (units: W m^{-2}); (d) SLP (units: hPa); (e) relative vorticity advection at 850 hPa (unit: 10^{-10} s^{-2}); and (f) vertical velocity at 850 hPa (units: 10^{-2} m s^{-1}). The dotted areas indicate that the differences are significant at a 95% level based on the *t*-test.

The proof of the impact of strong diurnal variation on the SMO does not depend on the selection of different indicators. Several indicators that represent the Asian SMO are selected to investigate the impact of strong diurnal variation on SMO, including the referenced panted rainfall rate defined by B. Wang and LinHo (2002), the tropospheric temperature gradient index defined by Xavier et al. (2007), and the Webster and Yang index defined by Webster and Yang (1992). These indicators are frequently used to determine the time of the SMO in terms of convection processes and large-scale monsoon circulation variations. All results demonstrate that the onset time of monsoon is advanced when strong diurnal variation is considered in Exp_SDA (*see* Figure S2 in in Supporting Information S1).

3.2. Physical Mechanism

Figure 3 presents the composite differences in multiple variables between Exp_SDA and Exp_WDA in the pre-onset stage. These differences provide insight into the impact of strong diurnal variation on the dynamic and thermodynamic processes related to SMO.

Strong diurnal variation contributes to a positive SST difference in the BoB, with a maximum difference increase by 0.5°C. In late April, SST warms up and typically exceeds 30°C from 10°N to 15°N before SMO (Yu, Li, et al., 2012), known as the spring warm pool of the BoB (Wu et al., 2012). This warm pool promotes convection activity and leads to the northward ISOs that significantly influence the formation of BoB SMO (K. Li, Li, et al., 2016; Wu et al., 2012). However, the intensity of the warm pool is underestimated in Exp_WDA compared with OISST. The warm center shifts southward, and the negative bias is dispersed from the north to the central BoB (Figure S3 in Supporting Information S1). Considering the effect of strong diurnal variation, SST rises in Exp_SDA, improving more than 50% cold bias in the central BoB. Meanwhile, surface air temperature at 2m (T2m) also warms before the SMO (Figure 3b), with a maximum difference distributed from the central BoB to the Andaman Islands.

Figure 3c shows the change in net heat flux induced by the strong diurnal effect. The upward direction is regarded as the positive direction. Thus, the negative heat flux anomalies spread from the central to the southwestern BoB, implying that more heat is absorbed by the ocean. In the pre-onset stage, a clear sky dominates over the BoB, resulting in stronger solar radiation absorption. The latent heat is restrained due to weak winds, rather than the changes of specific humidity difference, leading to the negative anomaly. Ocean surface warming promotes more heat release to the atmosphere, contributing to weak positive sensible and longwave radiation heat anomalies. From the perspective of heat flux transport, the combined effects of shortwave radiation and latent heat fluxes contribute to oceanic heat absorption (Figure S4 in Supporting Information S1). Meanwhile, the MLD is shallow and even decreases in the BoB due to the strong diurnal cycle (Figure S5 in Supporting Information S1), causing rapid heating of the ocean.

19448007, 2024, 15, Downloaded from https://agupubs.onlinelibrary.wiley.com/doi/10.1029/2023GL108015 by QINGDAO UNIVERSITY OF SCIENCE & TECH, Wiley Online Library on [09/03/2026]. See the Terms and Conditions (https://onlinelibrary.wiley.com/terms-and-conditions) on Wiley Online Library for rules of use; OA articles are governed by the applicable Creative Commons License

19448007, 2024, 15, Downloaded from https://agupubs.onlinelibrary.wiley.com/doi/10.1029/2023GL108015 by QINGDAO UNIVERSITY OF SCIENCE & TECH, Wiley Online Library on [09/03/2026]. See the Terms and Conditions (https://onlinelibrary.wiley.com/terms-and-conditions) on Wiley Online Library for rules of use; OA articles are governed by the applicable Creative Commons License

The diurnal variation not only influences the thermodynamics processes but also has significant impacts on atmospheric circulation. A low-pressure system forms in the southern BoB with an inverse pressure trough extending from the Andaman Sea to Burma (Figure 3d). The cyclonic circulation leads to positive relative vorticity advection (RVA) in the BoB (Figure 3e). Furthermore, the development of low-level trough is further promoted by the intensification of a high-pressure anomaly in the high-level atmosphere. Before the establishment of monsoon circulation, the South Asia high locates in the Indochina Peninsula and the South China Sea (Liu, Liu, et al., 2015). Our simulations suggest that the spatial distribution of this high-pressure system, represented by 200 hPa geopotential height, is reasonably simulated in Exp_SDA (Figure S6 in Supporting Information S1). Incorporation of the effect of strong diurnal also strengthens the high-pressure system from 500 to 850 hPa over the BoB and the South China Sea (Figures S7 and S8 in Supporting Information S1), contributing to the development of low-pressure trough in the low-levels atmosphere under the pumping action of the high-pressure system.

Strong diurnal variation promotes a local vertical air circulation, which is also conducive to SST warming. The downdraft indicated by positive vertical velocity anomaly distributes in the BoB, demonstrating that the BoB is dominated by fine weather under the control of a high-pressure system (Figure 3f). More solar radiation is absorbed by the ocean, so an increase in the amplitude of the diurnal variation will contribute to SST warming, until the SMO.

The development of low-pressure trough and positive RVA along the trough provide favorable conditions for the development of local convection and earlier SMO. Around 1 May, there is a negative bias of wind speed and a positive bias of OLR in Exp_WDA, indicating a delayed SMO with underestimated wind speed and overestimated OLR. By incorporating the strong diurnal variation effect, increased convective activity with more clouds blocks the OLR, leading to a negative difference in OLR between Exp_SDA and Exp_WDA (Figure S9 in Supporting Information S1). Results show that the wind speed is stronger in Exp_SDA, representing the advanced SMO. The simulation biases of wind speed and OLR are reduced by considering strong diurnal variation during SMO.

4. Conclusions and Discussion

The onset of monsoon, which signals the alternations of wet and dry seasons, is crucial for water resource management and socio-economic development. Despite advances in climate modeling, accurately simulating the onset time remains a challenge. The earliest signal of Asian SMO, known as the SMO in the BoB, is usually delayed by approximately 3–6 pentads in simulations. This is partly due to the models' inability to adequately capture high-frequency variability. Observations reveal that the strong diurnal variation occurs before the SMO. A strong diurnal cycle leads to warm SST and plays an important role in air-sea interactions related to SMO. Unfortunately, the diurnal intensity tends to be underestimated by the climate models.

A diagnostic sublayer scheme that realistically describes the diurnal amplitude was incorporated in FIO-ESM v2.0, resulting in the advance of 2–3 pentads in the time of SMO in the central BoB. Considering the strong diurnal variation, daily mean SST rises in the pre-onset stage (Figure 4a), leading to a warm pool that is more consistent with observations. Furthermore, local air circulation changes due to the warm underlying surface (Figure 4b). The cyclonic circulation develops in the low levels of the atmosphere, with the pressure trough distributed along the east coast of the BoB. In the middle to high levels of the atmosphere, a high-pressure system forms from the BoB to the South China Sea. Positive RVA along the trough is enhanced, which is conducive to the development of convective activity. In the vertical direction, a local air circulation with downdraft over the BoB and updraft over the land develops. Thus, the BoB is predominantly influenced by fair weather conditions, controlled by a high-pressure system. Enhanced absorption of solar radiation, suppressed latent heat release and shallow MLD contribute to an amplification in the diurnal variation, thereby facilitating SST warming until the SMO.

Previous studies show that the development of vortexes in the BoB and the northward propagation of ISOs trigger the SMO (K. Li, Li, et al., 2016; Wu et al., 2012). The SST warm pool provides necessary conditions for the development of vortexes and the movement of ISOs. However, it remains challenging for a climate model to simulate the formation of monsoon vortexes and the intensity and movement process of ISOs realistically, which even restricts the model's ability to accurately simulate the SMO. However, the local SST warming, leading to atmospheric instability and more convection activity, can be reasonably simulated by incorporating the diagnostic

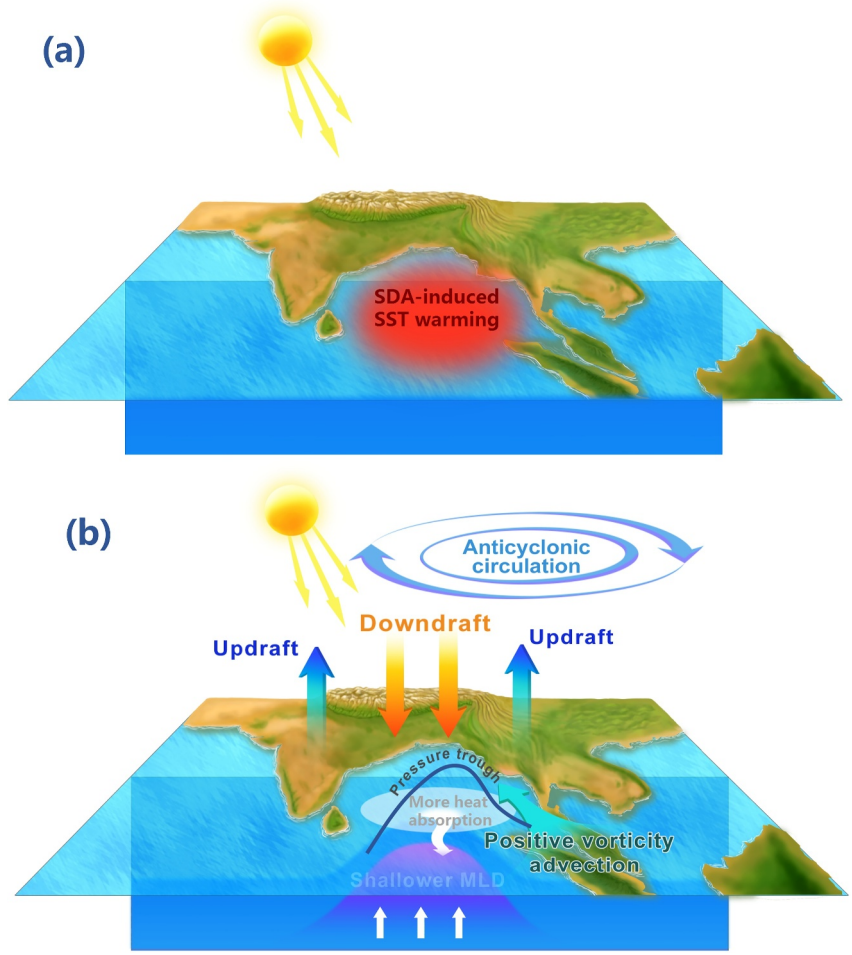

Figure 4. Schematic diagram of the influence of large diurnal amplitude on summer monsoon onset. (a) Sea surface temperature warms under the effects of large diurnal amplitude and (b) local air circulation changes due to the warm underlying surface. The development of the anticyclonic circulation in the high levels and the pressure trough in the low levels reinforces the downdraft and positive relative vorticity advection in the Bay of Bengal.

sublayer scheme. Accurate simulation of ocean warming depicts favorable large-scale environmental conditions that contribute to an advanced SMO.

Considering the strong diurnal variation can improve the delayed SMO bias in the central BoB. However, the relationship between the monsoon onset and the intensity of SST diurnal variation is nonlinear. The monsoon onset will not be infinitely advanced even if the diurnal variation intensifies many times. Besides, the delayed biases over the western BoB and the Andaman Sea have not been reduced. Further analysis of the physical processes is necessary as the monsoon processes involve multi-scale variability interactions.

Data Availability Statement

The experimental data of Exp_WDA and Exp_SDA are archived in the digital repository figshare (https://doi.org/10.6084/m9.figshare.24762369), which can be publicly accessed. RAMA data (McPhaden et al., 2009) are provided by the Global Tropical Moored Buoy Array (GTMBA) project office of NOAA/Pacific Marine Environmental Laboratory (https://www.pmel.noaa.gov/gtmba/pmel-theme/indian-ocean-rama). The NOAA OISST v2 data (Huang et al., 2021) are from https://psl.noaa.gov/data/gridded/data.noaa.oisst.v2.highres.html. ERA5 reanalysis data (Hersbach et al., 2020) are available at https://www.ecmwf.int/en/forecasts/dataset/ecmwf-reanalysis-v5. Daily NOAA interpolated OLR products (Chelliah & Arkin, 1992) are from https://www.ncei.noaa.gov/products/climate-data-records/outgoing-longwave-radiation-daily.

19448007, 2024, 15, Downloaded from https://agupubs.onlinelibrary.wiley.com/doi/10.1029/2023GL108015 by QINGDAO UNIVERSITY OF SCIENCE & TECH, Wiley Online Library on [09/03/2026]. See the Terms and Conditions (https://onlinelibrary.wiley.com/terms-and-conditions) on Wiley Online Library for rules of use; OA articles are governed by the applicable Creative Commons License

Acknowledgments
This work was jointly supported by the National Key R&D Program of China (2022YFF0802001), the Basic Scientific Fund for National Public Research Institute of China (Shu-Xingbei Young Talent Program 2023S01), the Marine S&T Fund of Shandong Province for Laoshan Laboratory (LSKJ202202100), the National Natural Science Foundation of China (42075039 and 42376033), the China-Korea Cooperation Project on Northwest Pacific Marine Ecosystem Simulation under the Climate Change. And we also thank for the Laoshan Laboratory providing the research fund.

References

Bao, Y., Song, Z., & Qiao, F. (2020). FIO-ESM version 2.0: Model description and evaluation. *Journal of Geophysical Research: Oceans*, *125*(6), e2019JC016036. https://doi.org/10.1029/2019JC016036

Bernie, D. J., Guilyardi, E., Madec, G., Slingo, J. M., Woolnough, S. J., & Cole, J. (2008). Impact of resolving the diurnal cycle in an ocean atmosphere GCM. Part 2: A diurnally coupled CGCM. *Climate Dynamics*, *31*(7–8), 909–925. https://doi.org/10.1007/s00382-008-0429-z

Bernie, D. J., Woolnough, S. J., Slingo, J. M., & Guilyardi, E. (2005). Modeling diurnal and intraseasonal variability of the ocean mixed layer. *Journal of Climate*, *18*(8), 1190–1202. https://doi.org/10.1175/JCLI3319.1

Branstetter, M. (2001). *Development of a parallel river transport algorithm and applications to climate studies*. University of Texas at Austin. Retrieved from https://repositories.lib.utexas.edu/handle/2152/10545

Chelliah, M., & Arkin, P. (1992). Large-scale interannual variability of monthly outgoing longwave radiation anomalies over the global tropics [Dataset]. *Journal of Climate*, *5*(4), 371–389. https://doi.org/10.1175/1520-0442(1992)005<0371:LSIVOM>2.0.CO;2

Craig, A. P., Vertenstein, M., & Jacob, R. (2011). A new flexible coupler for earth system modeling developed for CCSM4 and CESM1. *International Journal of High Performance Computing Applications*, *26*(1), 31–42. https://doi.org/10.1177/1094342011428141

Deepthi, B., & Sivakumar, B. (2022). General circulation models for rainfall simulations: Performance assessment using complex networks. *Atmospheric Research*, *278*, 106333. https://doi.org/10.1016/j.atmosres.2022.106333

Dong, G., Zhang, H., Moise, A., Hanson, L., Liang, P., & Ye, H. (2016). CMIP5 model-simulated onset, duration and intensity of the Asian summer monsoon in current and future climate. *Climate Dynamics*, *46*(1–2), 355–382. https://doi.org/10.1007/s00382-015-2588-z

Eyring, V., Bony, S., Meehl, G. A., Senior, C. A., Stevens, B., Stouffer, R. J., & Taylor, K. E. (2016). Overview of the coupled model intercomparison project phase 6 (CMIP6) experimental design and organization. *Geoscientific Model Development*, *9*(5), 1937–1958. https://doi.org/10.5194/gmd-9-1937-2016

Feng, J., Hu, D., & Yu, L. (2013). Role of western Pacific oceanic variability in the onset of the Bay of Bengal summer monsoon. *Advances in Atmospheric Sciences*, *30*(1), 219–234. https://doi.org/10.1007/s00376-012-2040-9

Gentemann, C. L., Minnett, P. J., & Ward, B. (2009). Profiles of ocean surface heating (POSH): A new model of upper ocean diurnal warming. *Journal of Geophysical Research*, *114*(C7), C07017. https://doi.org/10.1029/2008JC004825

He, J., & Zhu, Z. (2015). The relation of South China Sea monsoon onset with the subsequent rainfall over the subtropical East Asia. *International Journal of Climatology*, *35*(15), 4547–4556. https://doi.org/10.1002/joc.4305

Hersbach, H., Bell, B., Berrisford, P., Hirahara, S., Horányi, A., Sabater, M., et al. (2020). The ERA5 global reanalysis [Dataset]. *Quarterly Journal of the Royal Meteorological Society*, *146*(730), 1999–2049. https://doi.org/10.1002/qj.3803

Hu, D., Duan, A., Tang, Y., & Yu, W. (2023). Delayed onset of the tropical Asian summer monsoon in CMIP6 can be linked to the cold bias over the Tibetan Plateau. *Environmental Research Letters*, *18*(11), 114005. https://doi.org/10.1088/1748-9326/acff79

Huang, B., Liu, C., Banzon, V., Freeman, E., Graham, G., Hankins, B., et al. (2021). Improvements of the daily Optimum interpolation Sea Surface temperature (DOISST) version 2.1 [Dataset]. *Journal of Climate*, *34*(8), 2923–2939. https://doi.org/10.1175/JCLI-D-20-0166.1

Hunke, E. C., & Lipscomb, W. H. (2008). *CICE: The Los Alamos sea ice model. Documentation and software user's manual. Version 4.0*. Tech. Rep. LA-CC-06-012, T-3 fluid dynamics group. Los Alamos National Laboratory.

Lawrence, D. M., Oleson, K. W., Flanner, M. G., Thornton, P. E., Swenson, S. C., Lawrence, P. J., et al. (2011). Parameterization improvements and functional and structural advances in version 4 of the community land model. *Journal of Advances in Modeling Earth Systems*, *3*(1), M03001. https://doi.org/10.1029/2011MS00045

Li, J., Geen, R., Mao, J., Song, Y., Vallis, G. K., & Wu, G. (2023). Mechanical and thermal forcings of Asian large-scale orography on spring cloud amount and atmospheric radiation budget over East Asia. *Journal of Climate*, *36*(15), 1–37. https://doi.org/10.1175/JCLI-D-22-0797.1

Li, K., Li, Z., Yang, Y., Xiang, B., Liu, Y., & Yu, W. (2016). Strong modulations on the Bay of Bengal monsoon onset vortex by the first northward-propagating intra-seasonal oscillation. *Climate Dynamics*, *47*(1–2), 107–115. https://doi.org/10.1007/s00382-015-2826-4

Li, K., Liu, Y., Li, Z., Yang, Y., Feng, L., Khokiattiwong, S., et al. (2018). Impacts of ENSO on the Bay of Bengal summer monsoon onset via modulating the intraseasonal oscillation. *Geophysical Research Letters*, *45*(10), 5220–5228. https://doi.org/10.1029/2018GL078109

Li, K., Liu, Y., Yang, Y., Li, Z., Liu, B., Xue, L., & Yu, W. (2016). Possible role of pre-monsoon sea surface warming in driving the summer monsoon onset over the Bay of Bengal. *Climate Dynamics*, *47*(3–4), 753–763. https://doi.org/10.1007/s00382-015-2867-8

Li, Z., Xue, Y., Fang, Y., & Li, K. (2021). Modulation of environmental conditions on the significant difference in the super cyclone formation rate during the pre- and post-monsoon seasons over the Bay of Bengal. *Climate Dynamics*, *57*(9–10), 2811–2822. https://doi.org/10.1007/s00382-021-05840-7

Liu, B., Liu, Y., Wu, G., Yan, J., He, J., & Ren, S. (2015). Asian summer monsoon onset barrier and its formation mechanism. *Climate Dynamics*, *45*(3–4), 711–726. https://doi.org/10.1007/s00382-014-2296-0

Liu, B., Wu, G., & Ren, R. (2015). Influences of ENSO on the vertical coupling of atmospheric circulation during the onset of South Asian summer monsoon. *Climate Dynamics*, *45*(7–8), 1859–1875. https://doi.org/10.1007/s00382-014-2439-3

Mao, J., & Wu, G. (2007). Interannual variability in the onset of the summer monsoon over the eastern Bay of Bengal. *Theoretical and Applied Climatology*, *89*(3–4), 155–170. https://doi.org/10.1007/s00704-006-0265-1

Masson, S., Terray, P., Madec, G., Luo, J., Yamagata, T., & Takahashi, K. (2012). Impact of intra-daily SST variability on ENSO characteristics in a coupled model. *Climate Dynamics*, *39*(3–4), 681–707. https://doi.org/10.1007/s00382-011-1247-2

McPhaden, M. J., Meyers, G., Ando, K., Masumoto, Y., Murty, V. S. N., Ravichandran, M., et al. (2009). RAMA: The research moored array for African–Asian–Australian monsoon analysis and prediction [Dataset]. *Bulletin of the American Meteorological Society*, *90*(4), 459–480. https://doi.org/10.1175/2008BAMS2608.1

Neale, R. B., Chen, C.-C., Gettelman, A., Lauritzen, P. H., Park, S., Williamson, D. L., et al. (2010). Description of the NCAR community atmosphere model (CAM5.0). NCAR technical note TN-486+STR.

Qiao, F., Zhao, W., Yin, X., Huang, X., Liu, X., Shu, Q., et al. (2016). A highly effective global surface wave numerical simulation with ultra-high resolution. In *Proceedings of the international conference for high performance computing, networking, storage and analysis (SC '16)*. IEEE Press. https://doi.org/10.1109/SC.2016.4

Schiller, A., & Godfrey, J. S. (2005). A diagnostic model of the diurnal cycle of sea surface temperature for use in coupled ocean-atmosphere models. *Journal of Geophysical Research*, *110*(C11), C11014. https://doi.org/10.1029/2005JC002975

Shroyer, E., Tandon, A., Sengupta, D., Fernando, H. J. S. A., Lucas, J., Farrar, J. T. R., et al. (2021). Bay of Bengal intraseasonal oscillations and the 2018 monsoon onset. *Bulletin of the American Meteorological Society*, *102*(10), E1936–E1951. https://doi.org/10.1175/BAMS-D-20-0113.1

Smith, R., Jones, P., Briegleb, B., Bryan, F., Danabasoglu, G., Dennis, J., et al. (2010). The Parallel Ocean Program (POP) reference manual: Ocean component of the community climate system model (CCSM). Rep. LAUR-01853. Retrieved from http://n2t.net/ark:/85065/d70g3j4h

19448007, 2024, 15, Downloaded from https://agupubs.onlinelibrary.wiley.com/doi/10.1029/2023GL108015 by QINGDAO UNIVERSITY OF SCIENCE & TECH, Wiley Online Library on [09/03/2026]. See the Terms and Conditions (https://onlinelibrary.wiley.com/terms-and-conditions) on Wiley Online Library for rules of use; OA articles are governed by the applicable Creative Commons License

Soloviev, A., & Lukas, R. (1997). Observation of large diurnal warming events in the near-surface layer of the western equatorial Pacific warm pool. *Deep-Sea Research Part I*, *44*(6), 1055–1076. https://doi.org/10.1016/S0967-0637(96)00124-0

Song, Y. J., Li, X. F., Bao, Y., Song, Z. Y., Wei, M., Shu, Q., & Yang, X. D. (2020). FIO-ESM v2.0 outputs for the CMIP6 global monsoons model intercomparison project experiments. *Advances in Atmospheric Sciences*, *37*(10), 1045–1056. https://doi.org/10.1007/s00376-020-9288-2

Sperber, K. R., Annamalai, H., Kang, I. S., Kitoh, A., Moise, A., Turner, A., et al. (2013). The Asian summer monsoon: An intercomparison of CMIP5 vs. CMIP3 simulations of the late 20th century. *Climate Dynamics*, *41*(9–10), 2711–2744. https://doi.org/10.1007/s00382-012-1607-6

Wang, B., & LinHo. (2002). Rainy season of the Asian–Pacific summer monsoon. *Journal of Climate*, *15*(4), 386–398. https://doi.org/10.1175/1520-0442(2002)015<0386:RSOTAP>2.0.CO;2

Wang, B., Webster, P., Kikuchi, K., Yasunari, T., & Qi, Y. (2006). Boreal summer quasi-monthly oscillation in the global tropics. *Climate Dynamics*, *27*(7–8), 661–675. https://doi.org/10.1007/s00382-006-0163-3

Wang, H., Liu, F., & Dong, W. (2022). Features of climatological intraseasonal oscillation during Asian summer monsoon onset and their simulations in CMIP6 models. *Climate Dynamics*, *59*(11–12), 3153–3166. https://doi.org/10.1007/s00382-022-06223-2

Wang, X., Jiang, X., Yang, S., & Li, Y. (2013). Different impacts of the two types of El Niño on Asian summer monsoon onset. *Environmental Research Letters*, *8*(4), 44053. https://doi.org/10.1088/1748-9326/8/4/044053

Webster, P., & Yang, S. (1992). Monsoon and Enso: Selectively interactive systems. *Quarterly Journal of the Royal Meteorological Society*, *118*(507), 877–926. https://doi.org/10.1002/qj.49711850705

Wu, G., Guan, Y., Liu, Y., Yan, J., & Mao, J. (2012). Air–sea interaction and formation of the Asian summer monsoon onset vortex over the Bay of Bengal. *Climate Dynamics*, *38*(1–2), 261–279. https://doi.org/10.1007/s00382-010-0978-9

Wu, G., Guan, Y., Wang, T., Liu, Y., Yan, J., & Mao, J. (2011). Vortex genesis over the Bay of Bengal in spring and its role in the onset of the Asian summer monsoon. *Science China Earth Sciences*, *54*, 1–9. https://doi.org/10.1007/s11430-010-4125-6

Wu, G., Ren, S., Xu, J., Wang, D., Bao, Q., Liu, B., & Liu, Y. (2013). Impact of tropical cyclone development on the instability of South Asian High and the summer monsoon onset over Bay of Bengal. *Climate Dynamics*, *41*(9–10), 2603–2616. https://doi.org/10.1007/s00382-013-1766-0

Xavier, P., Marzin, C., & Goswami, B. (2007). An objective definition of the Indian summer monsoon season and a new perspective on the ENSO-monsoon relationship. *Quarterly Journal of the Royal Meteorological Society*, *133*(624), 749–764. https://doi.org/10.1002/qj.45

Yang, X., Bao, Y., Song, Z., Shu, Q., Song, Y., & Qiao, F. (2023). Key to ENSO phase-locking simulation: Effects of sea surface temperature diurnal amplitude. *npj Climate and Atmospheric Science*, *6*(1), 159. https://doi.org/10.1038/s41612-023-00483-3

Yang, X., Song, Z., Tseng, Y., Qiao, F., & Shu, Q. (2017). Evaluation of three temperature profiles of a sublayer scheme to simulate SST diurnal cycle in a global ocean general circulation model. *Journal of Advances in Modeling Earth Systems*, *9*(4), 1994–2006. https://doi.org/10.1002/2017MS000927

Yu, W., Li, K., Shi, J., Liu, L., Wang, H., & Liu, Y. (2012). The onset of the monsoon over the Bay of Bengal: The year-to-year variations. *Atmospheric and Oceanic Science Letters*, *5*(4), 342–347. https://doi.org/10.1080/16742834.2012.11447011

Yu, W., Shi, J., Liu, L., Li, K., Liu, Y., & Wang, H. (2012). The onset of the monsoon over the Bay of Bengal: The observed common features for 2008-2011. *Atmospheric and Oceanic Science Letters*, *5*(4), 314–318. https://doi.org/10.1080/16742834.2012.11447009

Zhu, Z., & He, J. (2013). The vortex over Bay of Bengal and its relationship with the outbreak of South China Sea summer monsoon. *Journal of Tropical Meteorology*, *29*(6), 915–923. https://doi.org/10.3969/j.issn.1004-4965.2013.06.005

Zhu, Z., & Li, T. (2017). Empirical prediction of the onset dates of South China Sea summer monsoon. *Climate Dynamics*, *48*(5–6), 1633–1645. https://doi.org/10.1007/s00382-016-3164-x

19448007, 2024, 15, Downloaded from https://agupubs.onlinelibrary.wiley.com/doi/10.1029/2023GL108015 by QINGDAO UNIVERSITY OF SCIENCE & TECH, Wiley Online Library on [09/03/2026]. See the Terms and Conditions (https://onlinelibrary.wiley.com/terms-and-conditions) on Wiley Online Library for rules of use; OA articles are governed by the applicable Creative Commons License